*J. Phys. Chem. A* **1999,** *103,* 2982−2991

# Microsolvation of $HN_2^+$ in Argon: Infrared Spectra and ab Initio Calculations of $Ar_n-HN_2^+$ ($n = 1-13$)

**Otto Dopfer,* Rouslan V. Olkhov, and John P. Maier**

*Institut für Physikalische Chemie, Universität Basel, Klingelbergstrasse 80, CH-4056 Basel, Switzerland*

*Received: December 16, 1998; In Final Form: February 22, 1999*

Infrared (IR) photodissociation spectra of mass selected $Ar_n-HN_2^+$ complexes ($n = 1-13$) have been recorded in the 4 $\mu$m spectral range in a tandem mass spectrometer. The dominant features are assigned to the $\nu_1 + m\nu_s$ ($m = 1, 2$) combination bands, where $\nu_1$ corresponds to the intramolecular N−H stretch mode and $\nu_s$ to the intermolecular stretching vibration of the first (proton-bound) Ar ligand. Systematic size-dependent complexation-induced frequency shifts and fragmentation branching ratios enabled the development of a consistent model for the cluster growth. The $Ar-HN_2^+$ dimer has a linear proton-bound structure and further Ar ligands fill two equatorial solvation rings around the linear dimer core, each of them containing up to five Ar atoms. The attachment of the 12th argon atom at the nitrogen end of $HN_2^+$ leads to the completion of the first solvation shell with an icosahedral structure. Weaker bands in the IR photodissociation spectra are attributed to less stable isomers. Comparison with previous studies of the related $Ar_n-HOSi^+$ and $Ar_n-HCO^+$ complexes reveals several similarities in the cluster growth. However, due to different charge distributions and anisotropies of the repulsive walls of the ionic cores, subtle differences occur in the order of shell filling as well as the occurrence and stability of isomeric structures. These differences are rationalized by two-dimensional intermolecular potential energy surfaces calculated at the MP2/aug-cc-pVTZ# level of theory.

## 1. Introduction

The solvation of ions with neutral ligands plays an important role in many areas of chemistry, physics, and biology.[1−4] Ion−neutral dimers are often intermediates of ion−molecule reactions.[5,6] The energetics and dynamics of many chemical reactions and other relaxation processes within isolated charged clusters (e.g., proton transfer, $S_N2$ reactions, caging) depend sensitively on the cluster size.[7−11] To rationalize these cluster phenomena, a detailed understanding of the interplay between the ion−ligand and ligand−ligand interactions is required. A plethora of thermochemical and mass spectrometric studies have established incremental ligand binding energies as a function of the cluster size, giving some insight into the cluster growth, e.g., the formation of solvation shells and the existence of isomers.[1,12]

It is well established that high-resolution spectroscopy provides direct experimental access to the intermolecular interaction potentials in weakly bound complexes.[13−17] In contrast to neutral clusters, less spectroscopic information is available for ionic complexes due to the difficulties encountered with the production of high number densities.[18−20] The high selectivity and sensitivity achieved by the combination of mass spectrometric and spectroscopic methods can overcome this problem, and it is mostly by photodissociation techniques that spectra of ionic complexes have been measured as a function of the cluster size.[19,21−23] Mass selection provides in these studies an elegant tool to follow the size-dependent properties of cluster ions from the monomer to the bulk. In this way, macroscopic bulk attributes can be related to the microscopic molecular properties.[24−26] To this end, systematic studies on size-selected clusters provide insight into the origin of matrix isolation and other solvation effects.[27]

Rare gas (Rg) atoms are the most simple ligands and often used as structureless probes for the investigation of intermolecular ion−ligand interactions in cluster ions. Various spectroscopic techniques have been employed to study the solvation of small cations and anions in argon. These include photodissociation in the IR (e.g., $CH_5^+$, $NH_4^+$, $HCO^+$, $HOSi^+$, and $CH_3^+$)[28−32] and UV/vis spectral ranges (e.g., $Sr^+$),[33] photodetachment (e.g., $Br^-$, $I^-$, and $O^-$),[24,34] and time-resolved pump−probe experiments (e.g., $I_2^-$).[10] Various cluster size dependent properties (spectral shifts, binding energies, electron affinities, etc.) probed in these spectroscopic studies showed pronounced discontinuities for certain cluster sizes, and these were related to the occurrence of distinct cluster geometries. For $Ar_n-M^\pm$ clusters with small $M^\pm$ ions, observed discontinuities at $n = 12$ have been interpreted as the closure of the first solvation shell, leading to a stable icosahedral structure.[35] This conclusion was confirmed by several theoretical approaches[36,37] as well as the observation of the magic number $n = 12$ in mass spectra of $Ar_n-M^\pm$ cluster ions, where M is either an atom or a small diatom (e.g., M = Ar, O, I, Mg, NO).[24,34,38−41] For $M^\pm$ ions with a size significantly larger than Ar (e.g., M = $(NO)_2$, $I_2$, $C_6H_6$),[10,39,41,42] the short-range repulsive interactions prevent the close approach necessary to form a close-packed icosahedron, and thus more than 12 Ar ligands are required to complete the first solvation shell.[40] In addition, some small open-shell ions (e.g., $C^+$) feature strongly directional intermolecular bonds to Ar ligands, thus also preventing the formation of regular icosahedral structures.[43]

In the present work, the microsolvation of $HN_2^+$ in Ar is compared to that of the previously studied $HCO^+$ and $SiOH^+$ systems.[30,31] All three ions are linear closed-shell species arising from the protonation of isovalent diatomic molecules. Moreover, $HCO^+$ and $HN_2^+$ are isoelectronic ions. The analysis of solvent-induced spectral shifts in IR photodissociation spectra of $Ar_n-$

---

* Corresponding author. E-mail: dopfer@ubaclu.unibas.ch.

10.1021/jp9847585 CCC: $18.00

$HCO^+$ and $Ar_n{-}HOSi^+$ cluster ions and the size-dependent photofragmentation branching ratios allowed to monitor the cluster growth, deduce structures and binding energies, and identify various isomers.[30,31] In the cases of $Ar{-}HCO^+$ and $Ar{-}HOSi^+$, ab initio calculations and high-resolution MW and IR spectra showed that both dimers possess linear proton-bound global minima.[30,31,44−46] Vibrational spectra of larger $Ar_n{-}HCO^+$ clusters revealed that further Ar ligands fill two equatorial solvation rings (containing up to five atoms) around the linear dimer core, with the 12th and terminal Ar atom completing the first solvation shell, leading to an icosahedral-like geometry.[30] In the case of $Ar_n{-}HOSi^+$, only spectra up to $n = 10$ have been obtained; however, the formation of solvation rings around the linear dimer core could also be deduced from the experimental and theoretical data.[31]

Induction interactions dominate the attractive part of the ion−ligand interactions in $Rg_n{-}M^{\pm}$ clusters where $M^{\pm}$ constitutes a closed-shell ion. The sequence of solvation shell filling will therefore be largely determined by the charge distribution in the respective molecular ion and the anisotropy arising from the repulsive wall.[34] As in $HCO^+$ the positive charge is mainly localized on the H and C atoms, the primary solvation ring in $Ar_n{-}HCO^+$ is located around the C−H bond and has thus contact with the proton-bound Ar ligand, while the second ring is positioned around the C−O bond.[30] Significant charge density on Si supports a second T-shaped $Ar{-}SiOH^+$ dimer (local minimum) with the Ar attached to the Si atom, which is only slightly less stable than the linear proton-bound dimer (global minimum). Consequently, in the most stable $Ar_n{-}HOSi^+$ clusters, the solvation ring centered around the Si atom of the dimer core is filled first; that is, this ring has no contact to the proton-bound Ar ligand.[31] Various less stable $Ar_n{-}HOSi^+$ complexes have also been identified (for certain $n$ values) from their IR spectral shifts, for example, those for $n < 4$ which have all Ar ligands in the first ring around Si, but none at the proton-bound site.[31]

In the present study, the microsolvation of $HN_2^+$ in argon is investigated by IR photodissociation spectroscopy of $Ar_n{-}HN_2^+$ complexes ($n = 1{-}13$). Part of the dimer spectrum has been analyzed previously,[47] and the relevant results are summarized in section 4.1.1. To complement the experimental approach, two-dimensional intermolecular potential energy surfaces for Ar bound to $HN_2^+$, $HCO^+$, and $HOSi^+$ have been calculated by ab initio methods, and these surfaces are then used to rationalize the experimental results for dimers and the larger clusters of these ions with Ar atoms.

## 2. Experimental Section

Infrared photodissociation spectra of mass-selected $Ar_n{-}HN_2^+$ complexes have been recorded in a tandem mass spectrometer described in detail elsewhere.[30,48] The cluster ion source comprises a pulsed supersonic expansion coupled to electron impact ionization. The employed gas mixture contained $N_2$, $H_2$, and Ar in a ratio of 1:20:300. Electron impact ionization is followed by ion−molecule reactions to produce $HN_2^+$. Cold $Ar_n{-}HN_2^+$ complexes were generated by subsequent three-body collisions. Figure 1 shows a mass spectrum of the ion source which reveals $Ar_n{-}HN_2^+$ as the dominant cluster ion series. All other complexes can be assigned to either $Ar_n{-}HN_{2k}^+$ ($k = 0, 2{-}5$) or $Ar_n{-}H_3^+$. The large amount of $H_2$ in the gas mixture led to mass spectra where almost all cluster ions were protonated species (e.g., no $Ar_n{-}N_{2k}^+$ ions were observed). The size distribution of $Ar_n{-}HN_2^+$ could be shifted to higher $n$ by increasing the stagnation pressure from 3 to 8 bar.

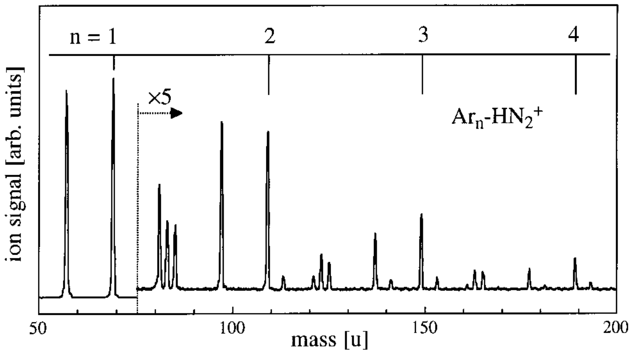

**Figure 1.** Part of the mass spectrum of the ion source demonstrating the efficient production of $Ar_n{-}HN_2^+$ complexes. Weaker cluster series include $Ar_n{-}HN_{2k}^+$ ($k = 0, 2{-}5$) and $Ar_n{-}H_3^+$.

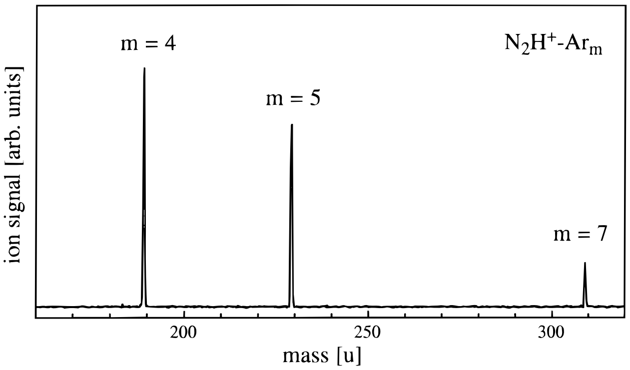

**Figure 2.** Mass spectrum obtained by scanning the second quadrupole mass spectrometer (QMS). The first QMS selected the $Ar_8{-}HN_2^+$ parent ion and the laser frequency was set to the resonance at 2618 $cm^{-1}$. $Ar_m{-}HN_2^+$ fragment ions with $m = 4$ and 5 arise from laser-induced dissociation (LID), while the ones with $m = 7$ are produced by collision-induced dissociation (CID) and/or metastable decomposition (MD).

Part of the plasma was extracted through a skimmer into the first quadrupole mass spectrometer (QMS) which was tuned to the mass of the desired $Ar_n{-}HN_2^+$ species. The mass-selected parent beam was then deflected by 90° and focused into an octopole ion guide, where it was exposed to the tunable IR laser pulse. Resonant excitation into metastable levels above the lowest dissociation limit caused the fragmentation of the parent ions into $Ar_m{-}HN_2^+$ and $(n - m)$ Ar atoms. The produced fragment ions were filtered by the second QMS and subsequently detected with a Daly-type cation detector.[49] Photofragmentation spectra were obtained by monitoring the fragment ion current as a function of the laser frequency.

For $Ar_n{-}HN_2^+$ clusters with $n > 1$, several fragment channels $m$ are possible following photoabsorption. In agreement with previous studies of related species, the range for $m$ was found to be small.[29−32,50] For example, resonant excitation of the mass selected $n = 8$ clusters at 2618 $cm^{-1}$ led only to the production of the $m = 4$ and 5 fragment ions (Figure 2). The $m = 7$ fragments arise not from laser-induced dissociation (LID) but from collision-induced dissociation (CID) with background gas and/or metastable decomposition (MD) of hot parent complexes in the octopole region. The CID and MD processes led mainly to $m = n - 1$ fragments. They interfered therefore only for small clusters with the LID signal, as larger complexes lost more than one ligand upon photoexcitation. To distinguish between LID and CID/MD processes, the source was triggered at twice the laser frequency and alternate signals were subtracted.

Tunable radiation in the mid-infrared spectral range (2500−6800 $cm^{-1}$) was generated by a pulsed optical parametric

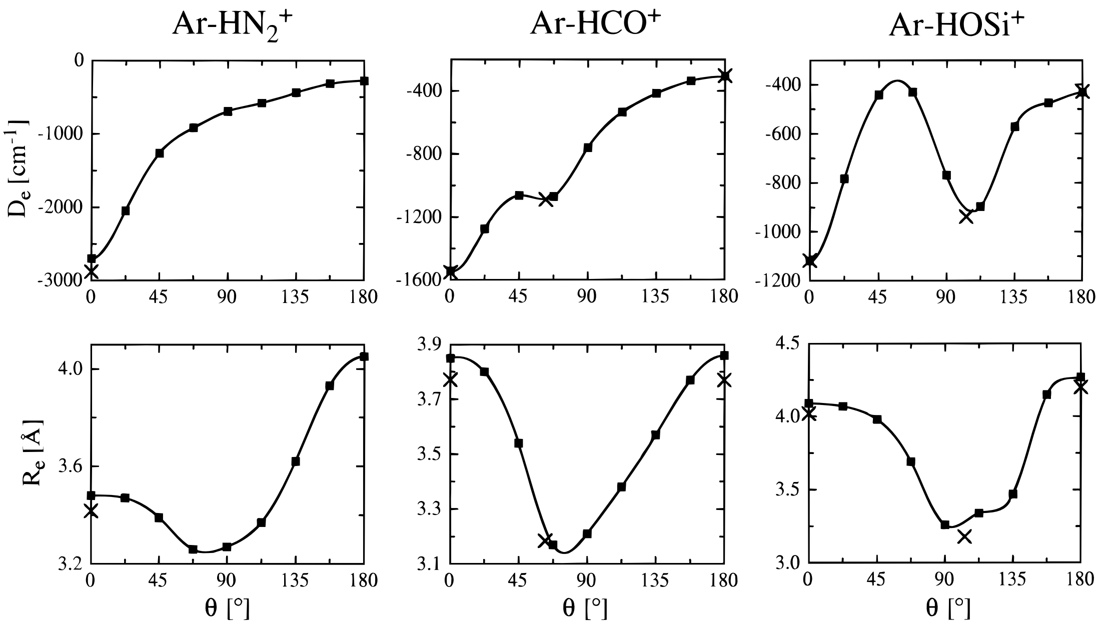

**Figure 3.** $D_e$ and $R_e$ values of one-dimensional radial cuts through the two-dimensional, intermolecular, rigid-monomer potential energy surfaces of Ar−HN$_2^+$ (left), Ar−HCO$^+$ (middle), and Ar−HOSi$^+$ (right), obtained at the MP2/aug-cc-pVTZ$^\#$ level of theory. The crosses correspond to calculations where the monomer coordinates were allowed to relax during the search for stationary points.

oscillator (OPO) based laser system with 0.02 cm$^{-1}$ bandwidth. The photofragmentation spectra were linearly normalized by laser power measured with an InSb detector. Calibration of the laser frequency was accomplished by comparison with simultaneously recorded optoacoustic spectra of N$_2$O.[51]

## 3. Ab Initio Calculations

Ab initio calculations at the MP2 level of theory were performed to determine the two-dimensional intermolecular potential energy surface of the Ar−HN$_2^+$ dimer. For comparison, the Ar−HCO$^+$ and Ar−HOSi$^+$ potentials have also been calculated at the same level of theory. The computations were conducted with the GAUSSIAN 94 program package[52] utilizing a basis set composed of Ahlrichs VTZ functions for the core electrons and diffuse and polarization functions taken from the aug-cc-pVTZ basis set.[53] This led to the following contraction scheme: (6s,3p,2d) → [4s,3p,2d] for H; (11s,7p,3d,2f) → [7s,4p,3d,2f] for C, N, and O; (13s,10p,3d,2f) → [8s,6p,3d,2f] for Si; (12s,10p,3d,2f) → [8s,6p,3d,2f] for Ar. This basis set, abbreviated in the present work as aug-cc-pVTZ$^\#$, is of similar quality as the aug-cc-pVTZ one and was shown to reliably reproduce the properties of proton-bound dimer interaction potentials.[46,54−56] Calculations at the HF level yielded substantially smaller binding energies due to the neglect of electron correlation, similar to calculations performed at the MP2 level with smaller basis sets.[29,32,57] As calculations for larger clusters at the MP2/aug-cc-pVTZ$^\#$ level are computationally much more expensive, the efforts have been limited to dimers in the present work.

To map the two-dimensional dimer intermolecular potential energy surfaces, interaction energies have been calculated for a grid of Jacobi coordinates $\theta$ and $R$. $\theta$ measures the angle between the vector $\vec{R}$, pointing from the center-of-mass of the core ion to the Ar atom, and the linear ion axis ($\theta = 0°$ for the proton-bound configuration). The structure of the ionic core was kept frozen at the optimized monomer geometry (rigid monomer approximation). Interaction energies were calculated for 9 values of $\theta$, equally spaced between 0 and 180°, and at least 10 radial points for each angle (spaced by 0.1 Å). All energies were corrected for basis set superposition error (BSSE).[58] One-dimensional radial cuts through the two-dimensional potential energy surfaces were created by cubic splines of the radial points along each angle, and their $R_e$ and $D_e$ values are plotted in Figure 3 as a function of $\theta$. Detailed data of the potential energy surfaces are available upon request.

To test the significance of the rigid monomer approximation, several stationary points have been calculated allowing all coordinates to relax (indicated by crosses in Figure 3). In these cases, the dissociation energy ($D_e$) was corrected for the relaxation energy arising from the monomer deformation upon complexation.[59] The effects of the rigid monomer approximation are most pronounced for the linear proton-bound global minimum structures ($\theta = 0°$, Figure 3 and Table 1). They lead to moderate underestimations in bond strengths (<7%) and bond lengths (<0.08 Å). Part of the discrepancy may also arise from the choice of the relatively large radial step size (0.1 Å) which causes errors via the splining procedure. In addition, the geometry optimizations were carried out on surfaces that are not corrected for BSSE, which usually leads to shorter bonds compared to BSSE-corrected surfaces.[60] The observed differences between the dimer surfaces with rigid and relaxed monomers are, however, small compared to the angular dependencies of the quantities $R_e$ and $D_e$. Thus, the rigid monomer surfaces are believed to be reliable semiquantitative representations of the intermolecular ion−ligand interactions, and they will be used below for the discussion of the properties of larger oligomers. It is noted that the theoretical results for the linear Ar−HCO$^+$ and Ar−HN$_2^+$ dimers compare favorably with existing calculations on these systems at similar levels of theory, adding confidence in the presented surfaces.[46,57]

To rationalize the topologies of the dimer potentials, charge and dipole moment distributions have been calculated using the "atoms in molecules" (AIM) analysis (Figure 4).[60−62] The AIM analysis was preferred over the Mulliken one, as the latter one depends sensitively on the basis set.[60,63] Indeed, in all cases the AIM multipole moments drastically deviated in magnitude and sometimes even in sign from those obtained with the Mulliken and natural bond orbital analysis. As can be seen from Figure

**TABLE 1: Geometries, Binding Energies, Harmonic Frequencies and IR Intensities (in km/mol, in Parentheses) of $ABH^+$ Ions ($AB = N_2$, SiO, and OC) and the Proton-Bound Global Minima of their Complexes with Ar Evaluated at the MP2/Aug-cc-pVTZ# Level[c]**

| species | | $r_{AB}$ [Å] | $r_{BH}$ [Å] | $r_{HAr}$ [Å] | $R_e$ [Å] | $D_e$ [cm$^{-1}$] | $\omega_1$ [cm$^{-1}$] | $\omega_2$ [cm$^{-1}$] | $\omega_3$ [cm$^{-1}$] | $\omega_s$ [cm$^{-1}$] | $\omega_b$ [cm$^{-1}$] |
|---|---|---|---|---|---|---|---|---|---|---|---|
| $N_2H^+$ | rel | 1.1058 | 1.0331 | | | | 3368.8 (652) | 720.8 (250) | 2144.4 (16) | | |
| $N_2H^+-Ar$ | rel | 1.1070 | 1.0838 | 1.8363 | 3.42 | 2880.5 | 2603.0 (2332) | 919.0 (144) | 2041.7 (753) | 209.7 (73) | 211.5 (35) |
| $N_2H^+-Ar$ | rig | 1.1058 | 1.0331 | 1.95 [b] | 3.48 [b] | 2699.3 | | | | | |
| $SiOH^+$ | rel[a] | 1.5500 | 0.9650 | | | | 3811 (596) | 424 (472) | 1127 (132) | | |
| $SiOH^+-Ar$ | rel[a] | 1.5477 | 0.9764 | 2.0990 | 4.02 | 1117 | 3555 (1826) | 662 (155) | 1141 (92) | 121 (26) | 87 (6) |
| $SiOH^+-Ar$ | rig | 1.5500 | 0.9650 | 2.20[b] | 4.09[b] | 1120 | | | | | |
| $OCH^+$ | rel | 1.1152 | 1.0899 | | | | 3260.6 (285) | 934.1 (34) | 2148.1 (40) | | |
| $OCH^+-Ar$ | rel | 1.1161 | 1.1090 | 2.0850 | 3.77 | 1551.4 | 2982.0 (1055) | 1080.6 (18) | 2111.8 (246) | 149.4 (46) | 170.9 (82) |
| $OCH^+-Ar$ | rig | 1.1152 | 1.0899 | 2.18[b] | 3.85[b] | 1543.1 | | | | | |

[a] Reference 31. [b] Uncertainty ca. 0.05 Å due to limited step size on the grid. [c] For the complexes the values are given for the rigid (rig) and relaxed (rel) monomers.

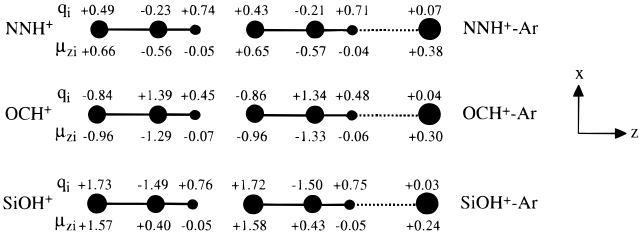

**Figure 4.** AIM charges ($q_i$ in $e$) and dipole moments ($\mu_{zi}$ in D) obtained for the $HN_2^+$, $HCO^+$, and $HOSi^+$ monomers and their linear complexes with Ar (relaxed monomers) calculated at the MP2/aug-cc-pVTZ# level.

4, there is only little charge transfer upon complexation. The strong dipoles induced on the Ar ligand reflect the important contributions of polarization interactions to the attractive part of the intermolecular potential. Moreover, there are large net dipole moments in the $HCO^+$ and $HOSi^+$ ions, whereas that of $HN_2^+$ is close to zero.

In addition to interaction energies and geometries, Table 1 lists harmonic vibrational frequencies and IR intensities for the monomers and the proton-bound dimers (with relaxed intramolecular coordinates). The most relevant results for the present study concern the X−H stretch vibration ($\omega_1$). This mode is for all monomers the vibration with highest IR oscillator strength. Complexation with Ar results in a large red shift of its frequency, accompanied by a strong increase of the IR intensity. These observations are typical for proton-bound dimers.[64] The properties of all stationary points found on the $Ar-HCO^+$ surface are compared in Table 2. The frequency and IR intensity of $\omega_1$ of $HCO^+$ are much less affected by Ar complexation in the antilinear and T-shaped geometries compared to the linear structure. These large differences clearly emphasize that vibrational spectra provide a very sensitive probe of the geometry and interaction strength in charged clusters.

A detailed comparison of the dimer potentials, multipole distributions, frequency shifts, and their effects on the cluster structures of the three considered cluster series is presented in section 4.2.

## 4. Experimental Results and Discussion

**4.1. $Ar_n-HN_2^+$ Spectra.** Figure 5 shows the mid-infrared photodissociation spectra of mass-selected $Ar_n-HN_2^+$ complexes ($n = 1-13$) recorded in the dominant fragment channels (indicated as $n \rightarrow m$). The centers and widths of the observed bands are summarized in Table 3.

*4.1.1. Dimer Spectrum ($n = 1$).* Part of the dimer spectrum has been analyzed previously and the relevant results can be summarized as follows.[47] Three rotationally resolved Σ−Σ type bands with band origins at 2755.6, 2707.3, and 2505.4 cm$^{-1}$ have been reported and their rotational analyses showed that they originate from the ground vibrational state of this linear proton-bound complex. The common feature of these bands was the lack of rotational lines terminating in levels below a certain $J'$ and this observation was explained by their stability against dissociation. The observed sudden onset in the photodissociation cross section allowed an accurate determination of the binding energy as $D_0 = 2781.5 \pm 1.5$ cm$^{-1}$, which is comparable to the calculated value $D_e = 2880.5$ cm$^{-1}$ (Table 1; $D_0 = 2800$ cm$^{-1}$ after including zero-point energies in the harmonic approximation). Analysis of the ground-state rotational constants resulted in a center-of-mass separation $R_0 = 3.429(4)$ Å and a harmonic intermolecular stretching frequency $\omega_s = 195(4)$ cm$^{-1}$ and force constant $k_s = 37.8(1.5)$ N/m,[47] in good agreement with the ab initio values in Table 1 and ref 57.

The vibrational assignment for the two strongest transitions at 2505.4 and 2755.6 cm$^{-1}$ as $\nu_1 + m\nu_s$ ($m = 1, 2$) was tentative and based on following arguments.[47] For the related $Rg-HCO^+$ and $Rg-HOCO^+$ series (Rg = He, Ne, Ar), a linear relation between the complexation-induced $\nu_1$ red shift ($\Delta\nu_1 = \nu_1^{\text{monomer}} - \nu_1^{\text{complex}}$) and the proton affinity (PA) of the Rg atom has been found.[64,65] Application of this rule to $Rg-HN_2^+$ gives an extrapolated $\nu_1$ frequency of 2280 cm$^{-1}$ for $Ar-HN_2^+$, implying a red shift of ∼950 cm$^{-1}$ from the monomer value (3233.95 cm$^{-1}$).[66] The harmonic red shift calculated in the present work amounts only to 766 cm$^{-1}$. But due to the strong interaction of the proton with the Ar ligand, the potential for the proton motion experiences a significant distortion upon Ar complexation. This effect causes large anharmonic corrections even for the fundamental frequency, and a one-dimensional anharmonic treatment resulted in $\nu_1 = 2330 \pm 100$ cm$^{-1}$.[57] The corresponding red shift of $900 \pm 100$ cm$^{-1}$ is in good agreement with the one obtained from the $\Delta\nu_1$ vs PA relation. As the $\nu_1$ fundamental is predicted to lie below the dissociation threshold of the complex, it cannot be observed in the present photodissociation experiment. High $J$ levels of the $\nu_1$ state are actually metastable with respect to dissociation; however, the transitions into these levels would (i) be very weak due to small thermal lower state populations and (ii) occur outside the scanning range of the employed laser system. Preliminary searches to locate the $\nu_1$ fundamental in the 2180−2410 cm$^{-1}$ range by direct IR absorption utilizing a tunable diode laser spectrometer combined with supersonic slit expansion failed so far, possibly due to the incomplete spectral coverage (with gaps up to 10 cm$^{-1}$) typical for laser diodes. The sensitivity of this technique should be sufficient to detect $\nu_1$, as the weaker $\nu_1 + \nu_s$ band at 2505.4 cm$^{-1}$ could be observed.[67,68]

The mid-infrared spectra of $He-HN_2^+$ and $Ne-HN_2^+$ feature strong transitions attributed to the $\nu_1$ fundamental of $HN_2^+$ and weaker transitions associated with combination bands of $\nu_1$ with

**TABLE 2: Geometries, Binding Energies, Harmonic Frequencies, and IR Intensities (in km/mol, in Parentheses) of Stationary Points on the Ar−HCO$^+$ Dimer Potential Energy Surface Evaluated at the MP2/Aug-cc-pVTZ$^\#$ Level**[c]

| structure[a] | $r_{OC}$ [Å] | $r_{CH}$ [Å] | $\theta$ | $R_e$ [Å] | $D_e$ [cm$^{-1}$] | $\omega_1$ [cm$^{-1}$] | $\omega_2$ [cm$^{-1}$] | $\omega_3$ [cm$^{-1}$] | $\omega_s$ [cm$^{-1}$] | $\omega_b$ [cm$^{-1}$] |
|---|---|---|---|---|---|---|---|---|---|---|
| linear (GM) $C_{\infty v}$ | 1.1161 | 1.1090 | 0° | 3.77 | 1551.4 | 2982.0 ($\sigma$/1055) | 1080.6 ($\pi$/18) | 2111.8 ($\sigma$/246) | 149.4 ($\sigma$/46) | 170.9 ($\pi$/82) |
| antilinear (TS) $C_{\infty v}$ | 1.1155 | 1.0896 | 180° | 3.77 | 303.6 | 3260.7 ($\sigma$/303) | 903.9 ($\pi$/36) | 2141.2 ($\sigma$/38) | 58.4 ($\sigma$/22) | −35.1 ($\pi$/74) |
| T-shaped[b] (LM) $C_s$ | 1.1156 | 1.0878 | ≈62° | ≈3.18 | 1088.8 | 3279.1 (a′/240) | 937.7 (a″/15)<br>895.4 (a′/5) | 2148.3 (a′/39) | 163.7 (a′/101) | 61.3 (a′/5) |

[a] GM = global minimum, TS = transition state, LM = local minimum. [b] ∠OCH = 178.6°, ∠CHAr = 86.1°. [c] All values are given for completely relaxed structures.

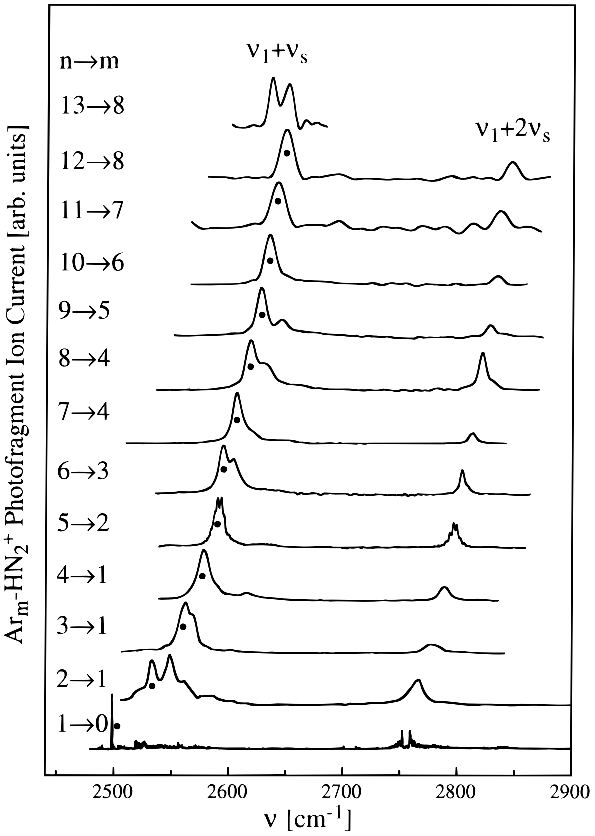

**Figure 5.** Mid-infrared photodissociation spectra of mass-selected Ar$_n$−HN$_2^+$ complexes ($n$ = 1−13) recorded in the dominant Ar$_m$−HN$_2^+$ fragment ion channel (indicated as $n \rightarrow m$). Although the spectra have been normalized for laser intensity variations assuming a linear power dependence, only the relative intensities of close-lying peaks are reliable. The dots indicate the $\nu_1 + \nu_s$ transition of the most stable isomer.

**TABLE 3: Band Centers and FWHM (in Parentheses) of Observed Transitions in the Photodissociation Spectra of Ar$_n$−HN$_2^+$ (→Ar$_m$−HN$_2^+$) in the Range of the $\nu_1 + \nu_s$ and $\nu_1 + 2\nu_s$ Bands**[b]

| $n$ | $m$ | $\nu_1 + \nu_s$ exptl | $\nu_1 + 2\nu_s$ exptl | $(\nu_1 + 2\nu_s) - (\nu_1 + \nu_s)$ exptl | $\nu_1$ ($\Delta\nu_1$) calcd |
|---|---|---|---|---|---|
| 1 | 0 | 2505.4 [a] | 2755.6[a] | 250.2 | 2255 (979) |
| 2 | 1 | 2533 (8)<br>2548 (8)<br>2522 (8)<br>2562 (10) | 2765 (10) | 232 | 2301 (933) |
| 3 | 1 | 2562 (10)<br>2568 (10) | 2778 (13) | 216 | 2346 (888) |
| 4 | 1 | 2578 (12) | 2788 (10) | 210 | 2368 (866) |
| 5 | 2 | 2591 (10) | 2797 (8) | 206 | 2385 (849) |
| 6 | 3 | 2594 (10)<br>2603 (10) | 2805 (7) | 211 | 2383 (851) |
| 7 | 4 | 2606 (7)<br>2614 (7) | 2813 (5) | 207 | 2399 (835) |
| 8 | 4 | 2618 (10)<br>2631 (10) | 2821 (6) | 203 | 2415 (819) |
| 9 | 5 | 2627 (8)<br>2646 (8) | 2828 (6) | 201 | 2426 (808) |
| 10 | 6 | 2634 (7)<br>2643 (8) | 2834 (7) | 200 | 2434 (800) |
| 11 | 7 | 2641 (9) | 2837 (7) | 196 | 2445 (789) |
| 12 | 8 | 2649 (8) | 2846 (7) | 197 | 2452 (782) |
| 13 | 8 | 2634 (6)<br>2650 (6) | | | |

[a] Band origins.[47] [b] For the most stable isomer the values for $(\nu_1 + 2\nu_s) - (\nu_1 + \nu_s)$ and the derived predictions for $\nu_1$ and $\Delta\nu_1$ in harmonic approximation are also listed. All values are given in cm$^{-1}$.

intermolecular bending ($\nu_b$) and stretching ($\nu_s$) modes.[56,69] Consequently, the strong Σ−Σ type transitions at 2505 and 2755 cm$^{-1}$ in the Ar−HN$_2^+$ spectrum were assigned to $\nu_1 + \nu_s$ and $\nu_1 + 2\nu_s$ combination bands. This results in an intermolecular stretching frequency of approximately 250 cm$^{-1}$, consistent with the ab initio calculations (Table 1 and ref 57) and the rotational constants of the involved vibrational levels.[70] Excitation of $\nu_1$ leads to a significant increase in the intermolecular interaction (indicated by the large $\nu_1$ red shift) due to the vibrationally enhanced proton transfer.[64] The intermolecular stretching frequency is therefore expected to increase upon $\nu_1$ excitation, which is compatible with the present assignment ($\omega_s \approx 200$ cm$^{-1}$ for $v_1 = 0$, and $\omega_s \approx 250$ cm$^{-1}$ for $v_1 = 1$). Though the assignments of the two considered bands to $\nu_1 + m\nu_s$ ($m$ = 1, 2) are not unambiguous, this interpretation is presently favored and will be used as the basis for the rest of this paper. The larger cluster spectra discussed below are compatible with such an assignment. (The most probable alternative interpretation as $\nu_1 + m\nu_s$, $m$ = 0 and 1, does not affect the conclusions derived below.) Strong anharmonic coupling between $\omega_1$ and $\omega_s$ may explain the large IR oscillator strengths of the $\nu_1 + m\nu_s$ combination bands observed in the dimer spectrum. A detailed account of the other transitions observed in the $n$ = 1 spectrum will be published separately.

*4.1.2. Larger Cluster Spectra (n = 2−13).* In contrast to the dimer, the photofragmentation spectra of larger Ar$_n$−HN$_2^+$ ($n$ = 2−13) complexes lack rotational structure, similar to previous observations for related systems.[30,31] Contour simulations for reasonable cluster geometries show that, at least for the trimer, the laser bandwidth of 0.02 cm$^{-1}$ should be sufficient to resolve individual rotational lines. Possible line broadening mechanisms include (i) homogeneous broadening due to rapid intracluster vibrational energy redistribution or predissociation and (ii) inhomogeneous broadening due to spectral congestion arising either from sequence hot bands involving low-frequency intermolecular modes or from the existence of several isomers.

The observed spectral shifts show a systematic dependence on the cluster size and thus provide information concerning the spectral assignments as well as cluster structures and relative stabilities of isomers. As can be seen from Figure 5, the two strongest features in each spectrum shift simultaneously by approximately the same amount in the same direction as the cluster size increases, supporting their assignment to $\nu_1 + m\nu_s$. The spectra of $n$ = 1−3 feature several other absorptions in

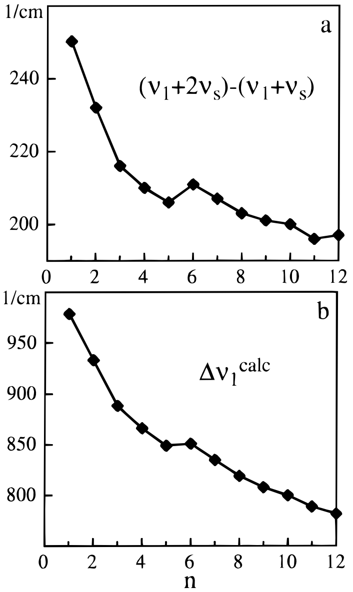

**Figure 6.** Plot of the measured spacings between the bands assigned to $\nu_1 + 2\nu_s$ and $\nu_1 + \nu_s$ in the $Ar_n-HN_2^+$ spectra as a function of the cluster size $n$ (a). Calculated $\nu_1$ red shifts obtained from $(\nu_1 + 2\nu_s)-(\nu_1 + \nu_s)$ assuming the harmonic approximation (b). For both plots only the most intense bands corresponding to the most stable isomers are considered.

the $\nu_1 + \nu_s$ range, which probably arise from further combination bands and/or overtones. They may gain intensity from $\nu_1 + \nu_s$ via a Fermi resonance, which would explain why the corresponding $\nu_1 + 2\nu_s$ range is less congested. For $n = 4-12$, the spectra are somewhat cleaner, possibly because the Fermi resonances in the $\nu_1 + \nu_s$ range are destroyed due to different spectral shifting of the interacting levels. These spectra feature only two strong absorptions that are associated with $\nu_1 + m\nu_s$ ($m = 1, 2$). As stated above, the combination bands $\nu_1 + m\nu_s$ have enhanced IR intensity due to strong anharmonic coupling, which is nearly independent of the cluster size. This supports cluster structures where the linear dimer core is only weakly perturbed by off-axis Ar ligands; that is, the $\nu_s$ mode in larger clusters corresponds mainly to a stretching vibration of the intermolecular bond to the first proton-bound Ar ligand.

Figure 6a shows the difference $(\nu_1 + 2\nu_s)-(\nu_1 + \nu_s)$ as a function of the cluster size $n$ (see also Table 3). In the harmonic approximation, this spacing corresponds to $\nu_s = \omega_s$ in the $v_1 = 1$ state. Subtracting this frequency from $\nu_1 + \nu_s$ gives an estimate for $\nu_1$, which in turn can be used to calculate the complexation-induced red shift, $\Delta\nu_1^{calc}$, as a function of the cluster size $n$ (Figure 6b). This procedure results in $\Delta\nu_1^{calc} = 979$ cm$^{-1}$ and $\omega_s = 250$ cm$^{-1}$ for the dimer, in good agreement with theoretical and thermochemical considerations outlined above. In Figure 5 and Table 3, the assignments of $\nu_1 + \nu_s$ for $n = 2$ and 3 were made so that a smooth and monotonic dependence for $\Delta\nu_1^{calc}$ is obtained in the size range $n = 1-5$. Such smooth dependencies were also observed for $Ar_n-HCO^+$ and $Ar_n-HOSi^+$.[30,31]

The direction and magnitudes of the spectral shifts deduced for $\nu_1$ and $\omega_s$ can be understood in following cluster growth model (Figure 7). The experimental and theoretical data demonstrate that the dimer ($n = 1$) has a linear proton-bound configuration. No other minimum has been located on the dimer potential energy surface. As the difference between the PA of $N_2$ and Ar is relatively small (124.6 kJ/mol),[71] complexation of $HN_2^+$ with Ar results in a strong intermolecular bond and a large $\nu_1$ red shift. Further Ar ligands cause the $\nu_1$ vibration to shift back to the blue, whereby the incremental shift, $\Delta\nu_1^{calc}(n) - \Delta\nu_1^{calc}(n - 1)$, is gradually decreasing from 46 cm$^{-1}$ ($n = 2$) to 7 cm$^{-1}$ ($n = 12$). (The predicted $\nu_1$ frequency for $n = 12$, $\nu_1^{calc} = 2452$ cm$^{-1}$, lies still below the scanning range of the employed OPO system.) Parallel to $\Delta\nu_1^{calc}$, the intermolecular stretching vibration decreases in the harmonic model from 250 cm$^{-1}$ ($n = 1$) to about 200 cm$^{-1}$ ($n = 12$) with a rate $\Delta\omega_s(n) = \omega_s(n)-\omega_s(n - 1)$ decreasing gradually from 18 cm$^{-1}$ ($n = 2$) to almost zero ($n = 12$). Thus, complexation of the $Ar-HN_2^+$ dimer core with further ligands weakens the intermolecular bond to the first Ar ligand (leading to a decrease in $\omega_s$), which in turn causes the N−H bond to become stronger again (indicated by the increase in $\nu_1^{calc}$).

The changes in $\omega_s$ and $\Delta\nu_1^{calc}$ are actually not monotonic in $n$ over the whole investigated size range (Figure 6). Discontinuities between $n = 5$ and 6 for both quantities are interpreted as a result of partial shell closing. The dimer potential has a deep minimum at the linear configuration indicating that sites with small $\theta$ are favorable in energy. Thus, further Ar ligands ($n = 2-5$) fill a solvation ring around the N−H bond of the linear dimer core. The observed discontinuities suggest that at $n = 6$ the second ring starts to be filled (Figure 7, bottom sequence). Four ligands in the first ring correspond to the coordination number six for the proton, which appears to be a stable configuration.[72]

Closer inspection of the spectra in Figure 5 reveals that for the size range $n = 6-10$ weaker satellite bands appear slightly to the blue of $\nu_1 + \nu_s$. Moreover, their positions follow smoothly and monotonically as a function of $n$ (without a discontinuity) those of the $\nu_1 + \nu_s$ absorptions for $n < 6$. These bands are attributed to the $\nu_1 + \nu_s$ transition of a less stable isomer. Based on a van der Waals radius of 1.85 Å for Ar,[13] the first ring is expected to be close to the calculated point on the dimer potential surface with $\theta = 67.5°$, $R_e = 3.26$ Å, and $D_e = 920$ cm$^{-1}$ (neglecting three-body effects; see below). For these structural parameters, four to five Ar ligands can fit into this ring. As a consequence, two isomers may coexist in the size range $n = 6-10$, one with four and the other one with five ligands in the first ring (Figure 7). In a later section it will be argued that the isomer with four Ar atoms in the first ring is the more stable one giving rise to the more intense $\nu_1 + \nu_s$ band (marked by dots in Figure 5). For $n = 12$ the first solvation shell is complete and the complex has a slightly distorted icosahedral geometry, with two Ar ligands on the $HN_2^+$ axis (at the H and N ends) and two five-membered solvation rings around the linear core (Figure 7). Only one $\nu_1 + \nu_s$ band is seen for $n = 12$ confirming that this isomer is significantly more stable than any other configuration.

Interestingly, two bands in the $\nu_1 + \nu_s$ range are again observed for $n = 13$. One features an incremental red shift of 15 cm$^{-1}$ suggesting that for this isomer the 13th Ar atom is close to the first ligand of the $Ar_{12}-HN_2^+$ icosahedron, thus producing the significant change in the $\nu_1$ and/or $\nu_s$ frequencies. At this site the attraction by the charge will force the 13th Ar ligand to slightly push on the proton-bound Ar, with the effect of strengthening the intermolecular bond and destabilizing the N−H bond. The almost unshifted band may be associated with isomeric structures having the 13th Ar atom further away from this sensitive position, i.e., between the two solvation rings or near the N end of $HN_2^+$.

As can be seen from Figure 6, the calculated $\nu_1$ frequency has not converged at $n = 12-13$. This indicates that the second and possibly also higher order solvation shells still provide significant contributions to the monomer-bulk shift. It appears that no Ar matrix isolation studies on $HN_2^+$ have been

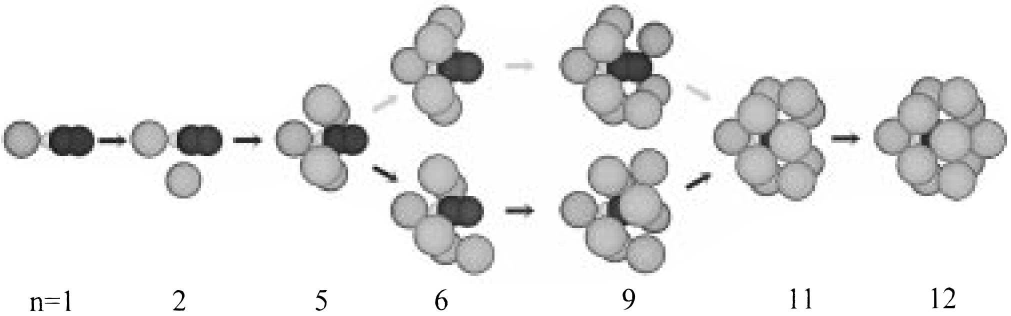

**Figure 7.** Sketch of isomeric geometries of $Ar_n-HN_2^+$ clusters. The bottom sequence corresponds to the most stable isomers. Isoelectronic $Ar_n-HCO^+$ complexes have similar structures.

performed, making it impossible at this stage to compare the cluster band shifts with the bulk limit. For $n = 12$, the absolute shift from the monomer value amounts to 24% of the monomer frequency, which is very large compared to usual vibrational shifts observed in Ar matrices (typically < 1.2%).[27] Incomplete shielding of the charge by the first solvation shell has also been observed in other ionic clusters systems.[24,25] Another reason for an unusually large shift for $\nu_1$ of $HN_2^+$ might be that this ion mainly exists as a proton-bound $Ar-HN_2^+$ dimer in the Ar environment.[27,73]

Two effects are considered to explain the direction and magnitudes of the shifts as a function of the cluster size: a "steric" and an "electronic" effect. The large $\nu_1$ red shift for the proton-bound dimer arises from a destabilization of the N−H bond upon formation of the linear proton bond. As the dimer potential has a deep minimum at $\theta = 0°$, the first solvation ring is expected to be close to the proton-bound Ar atom. This ring may slightly push on the proton-bound Ar atom, thus weakening this intermolecular bond and simultaneously stabilizing the N−H bond. As Ar ligands within the ring are roughly equivalent, the effect will be almost additive, resulting in nearly linear dependencies of $\nu_1$ and $\nu_s$ upon the number of atoms added to the ring. Members of the second ring may press on the first ring, which in turn pushes on the terminal ligand. Consequently, members of the second ring will cause effects similar to those of the first one, but they will be less pronounced due to the weaker bonds. Such a steric model, based on the subtle interplay between attractive and repulsive forces, was invoked in ref 30 to explain the $n$ dependencies of $\nu_1$ and $\nu_s$ in $Ar_n-HCO^+$ which parallel those of the isoelectronic $Ar_n-HN_2^+$ complexes.

The dimer potentials in Figure 3 suggest that changes in the electronic properties of the central ion may also provide some contribution to the observed solvation-induced frequency shifts. This will be outlined in more detail for the $Ar-HCO^+$ dimer, as its intermolecular potential surface features three stationary points (Figure 3 and Table 2): the linear global minimum ($\theta = 0°$, $D_e = 1551$ cm$^{-1}$), the T-shaped shallow local minimum ($\theta \approx 62°$, $D_e = 1089$ cm$^{-1}$), and the antilinear transition state ($\theta = 180°$, $D_e = 304$ cm$^{-1}$). Increasing $\theta$ from 0 to 180° causes the intermolecular bond to become weaker, whereby the $R_e$ dependence does not correlate with the $D_e$ dependence due to the anisotropy arising from the short-range repulsive forces (Figure 3). Approximating the $\nu_1$ normal mode by the C−H stretch local mode, the $\nu_1$ frequency is correlated with the C−H bond length. The harmonic shifts $\Delta\omega_1$ and $\Delta r_{CH}$ are calculated as $-278.6$, $+18.5$, and $+0.1$ cm$^{-1}$ and $+0.0191$, $-0.0021$, and $-0.0003$ Å for the linear, T-shaped, and antilinear structures, respectively (Tables 1 and 2). The experimental incremental shifts observed for $Ar_n-HCO^+$ amount to $-273.6$, $+30.6$, and $+3.2$ cm$^{-1}$ for $n = 1$, 2, and 12, respectively.[30] Thus, the magnitudes and directions of the $\nu_1$ shifts of the larger clusters can also be rationalized by the dimer potential, which reflects the dependence of the electronic structure of the $HCO^+$ ion upon the position of the Ar atom.

**4.2. Comparison of $Ar_n-HN_2^+$, $Ar_n-HCO^+$, and $Ar_n-HOSi^+$.** The interaction potentials of Ar bound to $HN_2^+$, $HCO^+$, and $HOSi^+$ reveal that all three complexes have a linear proton-bound global minimum structure. As the PA increases in the order $N_2$ < CO < SiO (493.8 < 594.0 < 777.8 kJ/mol),[71] the intermolecular bond strengths in the complexes of their protonated ions with Ar decrease in the same order. This effect is visible in the decreasing values for $D_e$, $k_s$, $\Delta\nu_1$, and $\Delta\omega_1$, and the increase in $R_{Ar-H}$ (Table 1, Figure 3, and Table 4 in ref 31). The calculated values are in good agreement with the spectroscopic data,[30,31,47] adding confidence to the quality of the calculated dimer potentials.

Although $N_2$, CO, and SiO are isovalent, the topologies of the surfaces in Figure 3 are quite different. While the $Ar-HN_2^+$ surface features only one deep linear proton-bound minimum, the potential of the isoelectronic $Ar-HCO^+$ complex has an additional shallow T-shaped local minimum ($\theta \approx 62°$). The $Ar-HOSi^+$ surface has also a second minimum, however this minimum occurs for a larger angle ($\theta \approx 103°$) and is more pronounced compared to $Ar-HCO^+$. The topologies of these surfaces can qualitatively be rationalized by considering the charge and dipole moment distributions in the respective ions (Figure 4) and the anisotropies arising from the repulsive walls (Figure 3). The attractive part of the potential is governed by the induction interaction of the atomic charges (and to lesser extent the atomic dipoles) of the ionic core with the induced dipole on Ar. In $HN_2^+$ the positive charge is mainly localized on the proton and the net dipole moment is close to zero. The charge-induced dipole interaction ($E_{cid}$), calculated with the point charges in Figure 4 at the respective equilibrium separations, strongly favors the linear dimer configuration ($E_{cid} \approx -4800$ cm$^{-1}$) over the antilinear one ($E_{cid} \approx -300$ cm$^{-1}$). The situation is very similar for $Ar-HCO^+$ where the point charges in $HCO^+$ again make the linear configuration much lower in energy than the antilinear one ($E_{cid} \approx -3150$ cm$^{-1}$ for $\theta = 0°$, $E_{cid} \approx -100$ cm$^{-1}$ for $\theta = 180°$). The large dipole moments on C and O pointing in the −z direction however slightly stabilize (destabilize) the antilinear (linear) structure, as they are parallel (antiparallel) to the induced dipole moment on Ar. In the case of $SiOH^+$, the atomic point charges contribute roughly equally to the binding energy at $\theta = 0$ and 180° ($E_{cid} \approx -800$ cm$^{-1}$), and it is the large atomic dipole moments on Si and O that stabilize the linear over the antilinear configuration. Thus, the induction interactions arising from the atomic multipole moments explain why all three cluster ions prefer the linear rather than the antilinear geometry. It also explains the decrease in binding energy for the proton-bound minimum in the series

$HN_2^+ > HCO^+ > HOSi^+$. The high positive charge densities on C in $HCO^+$ and on Si in $HOSi^+$ are responsible for the T-shaped local minima of the dimers. A detailed distributed multipole analysis[60,74] to quantitatively rationalize the dimer ab initio surfaces is, however, beyond the scope of this paper.

The dimer surfaces in Figure 3 will be used below to deduce the most stable structures of larger clusters and their isomers using the concept of pairwise additive interaction potentials. Such a procedure is only meaningful in cases where the three-body interaction terms are small compared to the anisotropy of the dimer ion−ligand potentials. The dominant three-body terms in charged complexes of ions surrounded by rare gas atoms arise from induction interactions.[34,60] The main term originates from the interaction of the dipole moments induced in two Ar ligands by the charge distribution on the core ion. Assuming that the two Ar ligands are separated by 3.75 Å (approximately the Ar−Ar separation in $Ar_2$)[13] and 3 Å away from a point charge, this repulsive three-body interaction term amounts to $\sim$50 $cm^{-1}$,[30] i.e., it is of the order of the attractive Ar−Ar van der Waals interaction[13] of $\sim$100 $cm^{-1}$, but much smaller than the angular variation of the binding energy $D_e$ in the dimer potentials in Figure 3. Thus, to a first approximation, three-body terms as well as ligand−ligand interactions can be neglected in developing coarse structures for the larger clusters.

In the previous section, the spectra of $Ar_n-HN_2^+$ complexes have been explained by global minimum structures where the first Ar atom occupies the linear proton-bound configuration and subsequent Ar ligands fill primary and secondary solvation rings around this dimer core, each containing up to five atoms. The solvation shell is then closed by the 12th Ar ligand at the N end (Figure 7). This scheme is supported by the dimer potential surface and the observed spectral frequency shifts. As the coarse topology of the $Ar-HCO^+$ dimer potential is similar to that of $Ar-HN_2^+$, the cluster growth should be analogous. Indeed, the spectral shifts in the $Ar_n-HCO^+$ spectra show the same behavior as for $Ar_n-HN_2^+$ supporting this conclusion. In the case of $Ar_n-HCO^+$, the relative spectral intensities of the less stable isomers (five Ar atoms in the first ring) compared to the more stable ones (four Ar atoms in the first ring) in the size range $n = 6-10$ are much lower than those of $Ar_n-HN_2^+$, indicating that it is energetically more difficult to fit five Ar atoms in the first ring around the $Ar-HCO^+$ core. This is supported by the ab initio dimer surfaces which show that the Ar atoms at $\theta \approx 65°$ are more strongly bound to $HCO^+$ than to $HN_2^+$ (with larger $D_e$ and smaller $R_e$ values), which may produce more steric hindrance for the fifth Ar atom to enter this ring.

The dimer potential of $Ar-HOSi^+$ differs from that of $Ar-HN_2^+$ and $Ar-HCO^+$ by having a second deep local minimum which is almost as stable as the global minimum. Indeed, the T-shaped dimer has been identified experimentally by its characteristic $\nu_1$ blue shift.[31] (In contrast, the T-shaped isomer of $Ar-HCO^+$ has not been identified in the experimental spectrum, probably due to its small isomerization barrier of <30 $cm^{-1}$ toward the linear configuration.) The existence of two deep minima on the dimer surface also determines the structures of larger clusters of $SiOH^+$ with Ar atoms. The most stable complexes for $n = 1-3$ have the first Ar atom in the linear configuration and further Ar ligands in a ring around the Si atom ($\theta \approx 103°$). A second, less stable isomer in this size range has all Ar atoms in this ring and no proton-bound one. Both isomers have been observed experimentally.[31] The most stable isomers up to $n \approx 10$ are formed by filling first a ring near the Si atom around the linear dimer core with five Ar atoms and then a second ring that is probably centered on the H−O bond. As Si has a larger radius than C, O, and N, five Ar atoms can easily fit into the first ring (in contrast to $HCO^+$ and $HN_2^+$). Thus, the $\nu_1$ shifts for the most stable isomer do not feature the discontinuity at $n = 6$ observed for $HCO^+$ and $HN_2^+$. However, a less stable isomer with four Ar atoms in the first ring has also been observed for $Ar_n-HOSi^+$ in the size range $n = 6-10$. Their $\nu_1$ shifts show a discontinuity at $n = 6$, similar to the most stable structures of $Ar_n-HCO^+$ and $Ar_n-HN_2^+$.

The first solvation ring in $Ar_n-HOSi^+$ has no contact with the proton-bound Ar ligand. Therefore, the $\nu_1$ shifts arise mainly from complexation-induced changes in the electronic structure of $SiOH^+$. In the case of $Ar_n-HCO^+$ and $Ar_n-HN_2^+$ both electronic and steric effects may operate. For $Ar_n-HCO^+$, the incremental $\nu_1$ shifts were almost constant within the two rings (25 and 4 $cm^{-1}$/ligand, respectively), whereas for $Ar_n-HOSi^+$ and $Ar_n-HN_2^+$ these shifts decrease significantly within each ring (34−12 and 5−0 $cm^{-1}$/ligand, and 46−17 and 16−11 $cm^{-1}$/ligand). This may tempt the speculation that nearly constant incremental shifts within one ring are related to steric effects, while decreasing ones may be related to electronic effects. If this rule holds, the frequency shifts are dominated by steric effects in $Ar_n-HCO^+$ and by electronic effects in $Ar_n-HN_2^+$ and $Ar_n-HOSi^+$. The local minimum in the $Ar-HCO^+$ dimer surface with a relatively short and strong bond close to the position of the first ring may force Ar ligands in this ring to push on the proton-bound Ar ligand in order to minimize the total energy, thus slightly destabilizing the intermolecular bond to the proton-bound Ar. In contrast, the $Ar-HN_2^+$ surface is quite flat near the angle $\theta$ for the first ring ($\theta \approx 65°$), causing less steric hindrance in $Ar_n-HN_2^+$ compared to $Ar_n-HCO^+$.

As was mentioned in the Introduction, $Ar_{12}-M^{\pm}$ cluster ions appear to have stable closed-shell icosahedral-like geometries only in cases where the size of the central $M^{\pm}$ ion is not significantly larger than that of an Ar atom. Approximating $HAB^+$ by $AB^+$ and the length of $AB^+$ by the sum of the van der Waals radii[75] of A and B plus the ab initio $r_{AB}$ separation, $HN_2^+$ and $HCO^+$ can fit inside a regular $Ar_{12}$ shell. In contrast, due to the large radius of Si, more than 12 Ar ligands may be necessary to close the first solvation shell in $Ar_n-HOSi^+$. Unfortunately, spectra of $Ar_n-HOSi$ have been recorded only for $n$ up to 10. Therefore, the question concerning the size of the first Ar solvation shell around $HOSi^+$ remains open.

**4.3. Comparison with $He_n-HN_2^+$, $Ne_n-HN_2^+$, and $(H_2)_n-HN_2^+$.** The spectra observed for $Ar_n-HN_2^+$ may be compared with those of $Ne_n-HN_2^+$ ($n = 1-5$)[56] and $He_n-HN_2^+$ ($n = 1,2$).[69] Due to weaker interactions in the Ne- and He-containing complexes, their investigations were limited to smaller cluster sizes. All three $Rg-HN_2^+$ dimers have linear proton-bound minima, and the interaction strengths scale with the proton affinity of the rare gas atoms ($D_e$ = 492, 896, and 2881 $cm^{-1}$ for He, Ne, and Ar). Accordingly, the observed $\nu_1$ red shifts of 76, 181, and $\sim$980 $cm^{-1}$ increase in the same order. A more detailed comparison of the structures, frequencies and intermolecular bond strengths of these three dimers may be found in refs 56 and 47.

In analogy to $Ar_n-HN_2^+$, for $Ne_n-HN_2^+$ and $He_n-HN_2^+$ the large red shifts in the $\nu_1$ frequency for $n = 1$ are contrasted by much smaller incremental blue shifts for clusters with $n > 1$. In the case of Ne, these shifts amount to $\sim$10 $cm^{-1}$ for $n = 2,3$ and $\sim$1−2 $cm^{-1}$ for $n = 4$, 5 and in the case of He the blue shift is 6 $cm^{-1}$ for $n = 2$.[56,69] These shifts suggest that the He- and Ne-containing complexes also grow around a linear $Rg-HN_2^+$ dimer core. However, as the interaction in the latter complexes is weaker than in the Ar-containing ones, their larger cluster structures may be less rigid. Consequently, the trend to form distinct primary and secondary solvation rings around the Rg$-$HN$_2^+$ dimer core may be less pronounced in the case of He and Ne ligands due to larger radial and angular delocalization. Moreover, as the van der Waals radii decrease in the order Ar $>$ Ne $>$ He (1.8 $>$ 1.2 $>$ 1.1 Å)[75] and the intermolecular separations to the HN$_2^+$ core are not too different for the three rare gas ligands,[54,56] more than 12 ligands may be necessary for closing the first solvation shell in the case of He and Ne.

The cluster structures of Ar$_n$$-$HN$_2^+$ may also be compared with those of (H$_2$)$_n$$-$HN$_2^+$.[72,76] The charge$-$quadrupole interaction arising from the positive quadrupole moment of H$_2$ and the positive charge on HN$_2^+$ favors a proton-bound T-shaped configuration for the H$_2$$-$HN$_2^+$ dimer, a conclusion that was confirmed by ab initio calculations and vibrational band shifts in the IR spectrum.[76] For larger clusters, no spectroscopic information is available. However, bond enthalpies determined from thermochemical studies on the clustering reaction (H$_2$)$_n$$-$HN$_2^+$ + H$_2$ $\rightarrow$ (H$_2$)$_{n+1}$$-$HN$_2^+$ and ab initio calculations suggested cluster geometries with a strongly bound T-shaped dimer core ($-\Delta H^0 = 9$ kcal/mol $\approx 2065$ cm$^{-1}$).[72] The next four ligands form a solvation ring around HN$_2^+$ leading to a stable structure with a six-fold coordination of the central proton, similar to the most stable structure suggested for Ar$_5$$-$HN$_2^+$. (H$_2$)$_n$$-$HN$_2^+$ geometries with $n > 6$ were argued to be more floppy than those for $n = 1-5$ with the sixth H$_2$ ligand completing the first solvation ring. In contrast to Ar$_n$$-$HN$_2^+$, where subsequent Ar atoms ($n > 6$) are believed to further solvate the HN$_2^+$ ion near the N end (Figure 7), H$_2$ ligands seem to prefer bonds to the first H$_2$ ligand.[72] This discrepancy may be attributed to the different nature of the intermolecular ion$-$ligand and ligand$-$ligand interactions and/or different ligand sizes in both complexes. Future IR spectroscopic work on (H$_2$)$_n$$-$HN$_2^+$ may shed some more light on their structures than is possible through thermodynamic studies. In these clusters, ligands can also be vibrationally excited and their frequency shifts have proven to be an extremely sensitive probe of their positions within the cluster.[50,77]

**4.4. Comparison with Ar$_n$$-$HF.** The Ar$_n$$-$HN$_2^+$ complexes may be compared with related neutral Ar-containing complexes, the best known system probably being Ar$_n$$-$HF.[15,78−82] Theoretical ($n = 1-14$) and high-resolution spectroscopic ($n = 1-4$) data revealed that the Ar$-$HF dimer also has a linear hydrogen-bonded equilibrium geometry. As the interaction in Ar$-$HF is considerably weaker than that in Ar$-$HN$_2^+$ ($D_0 = 101.7$ vs 2781.5 cm$^{-1}$), the Ar$-$H bond is significantly longer ($R_0 = 2.62$ vs 1.90 Å) and the complexation induced $\nu_1$ red shift is smaller (9.65 vs ~980 cm$^{-1}$). Due to the different interactions in both systems, the optimal structures of larger Ar$_n$$-$HF clusters differ largely from those of Ar$_n$$-$HN$_2^+$. HF points to the midpoint of an Ar$_2$ dimer for $n = 2$ (T-shaped, $C_{2v}$), to the center of a regular Ar$_3$ triangle for $n = 3$ ($C_{3v}$), and to the face of an Ar$_4$ tetrahedron for $n = 4$.[15] While in clusters up to $n = 8$ the HF molecule is bound to the surface of an Ar$_n$ microcluster, it is located inside of Ar$_n$ in larger systems. Ar$_{12}$$-$HF has a very stable icosahedral structure with an almost freely rotating HF unit at the center. The $\nu_1$ (H$-$F) red shifts directly reflect these Ar$_n$$-$HF minimum configurations.[81] The total red shift increases monotonically toward the bulk limit, which is already reached for $n = 12$, implying that for this system only the first solvation shell significantly contributes to the bulk shift.

Cluster structures similar to those of small Ar$_n$$-$HF complexes have previously also been invoked for Ar$_n$$-$HCO$^+$, with HCO$^+$ being located on the surface of an Ar$_n$ cluster and the O atom pointing toward its center.[83] However, such structures appear not to be compatible with the IR spectra of Ar$_n$$-$HCO$^+$ and Ar$_n$$-$HN$_2^+$, as they would not give rise to the observed $\nu_1$ shift dependencies. Thus, the different intermolecular forces acting in the neutral and charged systems lead to very different cluster structures, at least for those with a small number of ligands.

**TABLE 4: Photofragmentation Branching Ratios for the Reaction Ar$_n$$-$HN$_2^+$ + $h\nu$ $\rightarrow$ Ar$_m$$-$HN$_2^+$ + ($n - m$)Ar, Measured at the Peak Maxima of the $\nu_1 + \nu_s$ Band of the Most Stable Isomer[a]**

| $n$ | 1 | 2 | 3 | 4 | 5 | 6 | 7 | 8 | 9 | 10 | 11 | 12 |
|---|---|---|---|---|---|---|---|---|---|---|---|---|
| $m$ | 0 (1.0) | 1 (1.0) | 1 (1.0) | 1 (0.61)<br>2 (0.39) | 1 (0.02)<br>2 (0.73)<br>3 (0.25) | 2 (0.02)<br>3 (0.94)<br>4 (0.04) | 4 (1.0) | 4 (0.60)<br>5 (0.40) | 5 (1.0) | 5 (0.04)<br>6 (0.96) | 6 (0.21)<br>7 (0.79) | 7 (0.04)<br>8 (0.96) |
| $\langle n - m \rangle$ | 1.0 | 1.0 | 2.0 | 2.61 | 2.77 | 3.02 | 3.0 | 3.60 | 4.0 | 4.04 | 4.21 | 4.04 |

[a] Uncertainties are estimated as 0.05. The average number of Ar ligands lost ($\langle n - m \rangle$) is also given.

**4.5. Branching Ratios and Binding Energies.** Photoexcitation of Ar$_n$$-$HN$_2^+$ parent clusters at their $\nu_1 + \nu_s$ band maxima led to the observation of several Ar$_m$$-$HN$_2^+$ ($m < n$) fragment channels. Similar to previous studies of related systems, the range of $m$ was quite small for a given $n$ (Table 4). This information can be used to provide a rough estimate of incremental binding energies, $D_0(n)$. Neglecting kinetic energy release and differences in internal energies of parent and daughter ions, the absorbed photon energy must be larger than the sum of the binding energies of the evaporated Ar ligands.[84,85] Under the additional assumption that Ar ligands within one ring have the same bond strengths, the following limits for incremental binding energies have been derived: $D_0 > 2600$ cm$^{-1}$ for $n = 1$, 650 cm$^{-1}$ $< D_0 <$ 870 cm$^{-1}$ for $n = 2-6$ (first ring), and 520 cm$^{-1}$ $< D_0 <$ 650 cm$^{-1}$ for $n = 7-11$ (second ring). These values may be compared with the experimental binding energy $D_0 = 2781.5 \pm 1.5$ cm$^{-1}$ ($n = 1$)[47] and the theoretical values extracted from the dimer surface in Figure 3 of $D_e = 2699$ cm$^{-1}$ for $n = 1$, 916 cm$^{-1}$ for $n = 2-6$ ($\theta = 67.5°$, approximate position of first ring), and 442 cm$^{-1}$ for $n = 7-11$ ($\theta = 135.0°$, approximate position of the second ring). The approximations involved in the different methods for the determination of the incremental binding energies prevent better quantitative agreement; however, the qualitative agreement may be regarded as further support for the microsolvation model developed from the spectroscopic data.

## 5. Conclusions

The microsolvation of HN$_2^+$ ions in argon has been investigated by IR photodissociation spectroscopy of mass-selected Ar$_n$$-$HN$_2^+$ ($n = 1-13$) complexes. The analysis of systematic size-dependent spectral shifts and fragmentation branching ratios enabled the development of a consistent cluster growth scheme, including the identification of shell formation and existence of less stable isomers. The derived cluster structures are compatible with the two-dimensional intermolecular dimer potential energy surface calculated at the MP2 level of theory. Comparison with other charged and neutral Rg$_n$$-$M$^{(\pm)}$ cluster series revealed that the microsolvation process sensitively depends on the nature of the solute$-$solvent and solvent$-$solvent interactions (type and strength of the interactions, the charge distributions on the central core, the sizes of the solute and solvent molecules, etc.).

Most similarities have been found for the structures of the isoelectronic $Ar_n-HN_2^+$ and $Ar_n-HCO^+$ species. Hopefully, high-level ab initio calculations on larger oligomers will soon become feasible and allow inclusion of the effects of three-body interactions, zero-point energies, and entropy. The most promising experimental methods for further investigations of the structure and dynamics of small $Ar_n-HN_2^+$ complexes appear to be microwave or far IR spectroscopy in slit jets, as with these spectroscopic techniques stable rovibrational levels of these strongly bound complexes can be probed at high resolution.[45]

**Acknowledgment.** This study is part of the project 20-49104.96 of the Swiss National Science Foundation. The authors thank D. Roth for experimental assistance. O.D. thanks J. Cioslowski (Florida State University) for fruitful discussions concerning the interpretation of AIM multipole moments.

## References and Notes

(1) Castleman, A. W. In *Clusters of Atoms and Molecules II*; Haberland, H., Ed.; Springer: Berlin, 1994; p 77.

(2) Castleman, A. W.; Bowen, K. H. *J. Phys. Chem.* **1996**, *100*, 12911.

(3) Anderson, S. L. In *Clusters of Atoms and Molecules II*; Haberland, H., Ed.; Springer: Berlin, 1994; p 241.

(4) Hobza, P.; Zahradnik, R. *Intermolecular Complexes: The Role of van der Waals Systems in Physical Chemistry and in the Biodisciplines*; Elsevier: Amsterdam, 1988.

(5) Hase, W. L.; Wang, H.; Peslherbe, G. H. In *Advances in Gas-Phase Ion Chemistry*; Adams, N. G., Babcock, L. M., Ed.; JAI: Greenwich, 1998; Vol. 3; p 125.

(6) Bowen, R. D. *Acc. Chem. Res.* **1991**, *24*, 364.

(7) Castleman, A. W., Jr., In *Advances in Gas-Phase Ion Chemistry*; Adams, N. G., Babcock, L. M., Ed.; JAI: Greenwich, 1998; Vol. 3; p 185.

(8) Castleman, A. W.; Wei, S. *Annu. Rev. Phys. Chem.* **1994**, *45*, 685.

(9) Brutschy, B. *Chem. Rev.* **1992**, *92*, 1567.

(10) Vorsa, V.; Campagnola, P. J.; Nandi, S.; Larsson, M.; Lineberger, W. C. *J. Chem. Phys.* **1996**, *105*, 2298.

(11) Choi, J. H.; Kuwata, K. T.; Haas, B. M.; Cao, Y.; Johnson, M. S.; Okumura, M. *J. Chem. Phys.* **1994**, *100*, 7153.

(12) Lifshitz, C. In *Cluster Ions*; Ng, C. Y., Baer, T., Powis, I., Ed.; Wiley: New York, 1993; p 121.

(13) Hutson, J. M. *Annu. Rev. Phys. Chem.* **1990**, *41*, 123.

(14) Cohen, R. C.; Saykally, R. J. *J. Phys. Chem.* **1992**, *96*, 1024.

(15) Nesbitt, D. J. *Annu. Rev. Phys. Chem.* **1994**, *45*, 367.

(16) Leopold, K. R.; Fraser, G. T.; Novick, S. E.; Klemperer, W. *Chem. Rev.* **1994**, *94*, 1807.

(17) van der Avoird, A.; Wormer, P. E. S.; Moszynski, R. *Chem. Rev.* **1994**, *94*, 1931.

(18) Castleman, A. W.; Keesee, R. G. *Chem. Rev.* **1986**, *86*, 589.

(19) Bieske, E. J.; Maier, J. P. *Chem. Rev.* **1993**, *93*, 2603.

(20) Müller-Dethlefs, K.; Dopfer, O.; Wright, T. G. *Chem. Rev.* **1994**, *94*, 1845.

(21) Duncan, M. A. *Annu. Rev. Phys. Chem.* **1997**, *48*, 69.

(22) Lisy, J. M. In *Cluster Ions*; Ng, C.-Y., Baer, T., Powis, I., Ed.; Wiley: New York, 1993; p 217.

(23) Crofton, M. W.; Price, J. M.; Lee, Y. T. In *Clusters of Atoms and Molecules II*; Haberland, H., Ed.; Springer: Berlin, 1994; p 44.

(24) Arnold, S. T.; Hendricks, J. H.; Bowen, K. H. *J. Chem. Phys.* **1995**, *102*, 39.

(25) Jortner, J. *Z. Phys. D* **1992**, *24*, 247.

(26) Rips, I.; Jortner, J. *J. Chem. Phys.* **1992**, *97*, 536.

(27) Jacox, M. E. *Chem. Phys.* **1994**, *189*, 149.

(28) Boo, D. W.; Lee, Y. T. *Int. J. Mass. Spectrom. Ion Processes* **1996**, *159*, 209.

(29) Dopfer, O.; Nizkorodov, S. A.; Meuwly, M.; Bieske, E. J.; Maier, J. P. *Int. J. Mass Spectrom. Ion Processes* **1997**, *167−168*, 637.

(30) Nizkorodov, S. A.; Dopfer, O.; Ruchti, T.; Meuwly, M.; Maier, J. P.; Bieske, E. J. *J. Phys. Chem.* **1995**, *99*, 17118.

(31) Olkhov, R. V.; Nizkorodov, S. A.; Dopfer, O. *Chem. Phys.* **1998**, *239*, 393.

(32) Olkhov, R. V.; Nizkorodov, S. A.; Dopfer, O. *J. Chem. Phys.* **1998**, *108*, 10046.

(33) Fanourgakis, G. S.; Farantos, S. C.; Lüder, C.; Velegrakis, M.; Xantheas, S. S. *J. Chem. Phys.* **1998**, *109*, 108.

(34) Yourshaw, I.; Zhao, Y.; Neumark, D. M. *J. Chem. Phys.* **1996**, *105*, 351.

(35) Mackay, A. L. *Acta Crystallogr.* **1962**, *15*, 916.

(36) Hoare, M. R. *Adv. Chem. Phys.* **1979**, *40*, 49.

(37) Böhmer, H. U.; Peyerimhoff, S. D. *Z. Phys. D* **1989**, *11*, 239.

(38) Harris, I. A.; Kidwell, R. S.; Northby, J. A. *Phys. Rev. Lett.* **1984**, *53*, 2390.

(39) Stace, A. J. *Chem. Phys. Lett.* **1985**, *113*, 355.

(40) Prekas, D.; Lüder, C.; Velegrakis, M. *J. Chem. Phys.* **1998**, *108*, 4450.

(41) Desai, S. R.; Feigerle, C. S.; Miller, J. C. *J. Chem. Phys.* **1992**, *97*, 1793.

(42) Guillaume, C.; Le Calve, J.; Dimicoli, I.; Mons, M. *Z. Phys. D* **1994**, *32*, 157.

(43) Froudakis, G. E.; Fanourgakis, G. S.; Farantos, S. C.; Xantheas, S. S. *Chem. Phys. Lett.* **1998**, *294*, 109.

(44) Linnartz, H.; Speck, T.; Maier, J. P. *Chem. Phys. Lett.* **1998**, *288*, 504.

(45) Ohshima, Y.; Sumiyoshi, Y.; Endo, Y. *J. Chem. Phys.* **1997**, *106*, 2977.

(46) Nowek, A.; Leszczynski, J. *J. Chem. Phys.* **1996**, *105*, 6388.

(47) Nizkorodov, S. A.; Spinelli, Y.; Bieske, E. J.; Maier, J. P.; Dopfer, O. *Chem. Phys. Lett.* **1997**, *265*, 303.

(48) Bieske, E. J. *J. Chem. Soc., Faraday Trans.* **1995**, *91*, 1.

(49) Daly, N. R. *Rev. Sci. Instrum.* **1960**, *31*, 264.

(50) Okumura, M.; Yeh, L. I.; Lee, Y. T. *J. Chem. Phys.* **1988**, *88*, 79.

(51) Guelachvili, G.; Rao, K. N. *Handbook of Infrared Standards*; Academic Press: London, 1993; Vols. 1 and 2.

(52) Frisch, M. J.; Trucks, G. W.; Schlegel, H. B.; Gill, P. M. W.; Johnson, B. G.; Robb, M. A.; Cheeseman, J. R.; Keith, T.; Petersson, G. A.; Montgomery, J. A.; Raghavachari, K.; Al-Laham, M. A.; Zakrzewski, V. G.; Ortiz, J. V.; Foresman, J. B.; Cioslowski, J.; Stefanov, B. B.; Nanayakkara, A.; Challacombe, M.; Peng, C. Y.; Ayala, P. Y.; Chen, W.; Wong, M. W.; Andres, J. L.; Replogle, E. S.; Gomperts, R.; Martin, R. L.; Fox, D. J.; Binkley, J. S.; Defrees, D. J.; Baker, J.; Stewart, J. P.; Head-Gordon, M.; Gonzales, C.; Pople, J. A. *GAUSSIAN 94*, Revision B.2./E.2.; Gaussian, Inc: Pittsburgh, PA, 1995.

(53) Extensible Computational Chemistry Environmental Basis Set Data Base, version 10, 1996.

(54) Meuwly, M.; Bemish, R. J. *J. Chem. Phys.* **1997**, *106*, 8672.

(55) Meuwly, M.; Maier, J. P.; Rosmus, P. *J. Chem. Phys.* **1998**, *109*, 3850.

(56) Nizkorodov, S. A.; Meuwly, M.; Maier, J. P.; Dopfer, O.; Bieske, E. J. *J. Chem. Phys.* **1998**, *108*, 8964.

(57) Kolbuszewski, M. *Chem. Phys. Lett.* **1995**, *244*, 39.

(58) Boys, S. F.; Bernardi, F. *Mol. Phys.* **1970**, *19*, 553.

(59) Chalasinski, G.; Szczesniak, M. M. *Chem. Rev.* **1994**, *94*, 1.

(60) Stone, A. J. *The theory of intermolecular forces*; Clarendon Press: Oxford, 1996; p 264.

(61) Bader, R. F. W. *Atoms in molecules: a quantum theory*; Clarendon Press: Oxford, 1990.

(62) Cioslowsky, J. *Chem. Phys. Lett.* **1992**, *194*, 73.

(63) Cioslowski, J.; Hay, P. J.; Ritchie, J. P. *J. Phys. Chem.* **1990**, *94*, 148.

(64) Dopfer, O.; Olkhov, R. V.; Roth, D.; Maier, J. P. *Chem. Phys. Lett.* **1998**, *296*, 585.

(65) Nizkorodov, S. A.; Dopfer, O.; Meuwly, M.; Maier, J. P.; Bieske, E. J. *J. Chem. Phys.* **1996**, *105*, 1770.

(66) Kabbadj, Y.; Huet, T. R.; Rehfuss, B. D.; Gabrys, C. M.; Oka, T. *J. Mol. Spectrosc.* **1994**, *163*, 180.

(67) Speck, T.; Linnartz, H.; Maier, J. P. *J. Chem. Phys.* **1997**, *107*, 8706.

(68) Speck, T. Ph.D. Thesis, University of Basel, 1998.

(69) Meuwly, M.; Nizkorodov, S. A.; Maier, J. P.; Bieske, E. J. *J. Chem. Phys.* **1996**, *104*, 3876.

(70) Nizkorodov, S. A. Ph.D. Thesis, University of Basel, 1997.

(71) Hunter, E. P. L.; Lias, S. G. *J. Phys. Chem. Ref. Data* **1998**, *27*, 413.

(72) Hiraoka, K.; Katsuragawa, J.; Minamitsu, A.; Ignacio, E. W.; Yamabe, S. *J. Phys. Chem. A* **1998**, *102*, 1214.

(73) Lugez, C. L.; Jacox, M. E.; Johnson, R. D., III *J. Chem. Phys.* **1999**, *110*, 5037.

(74) Stone, A. J. *Chem. Phys. Lett.* **1981**, *83*, 233.

(75) Badenhoop, J. K.; Weinhold, F. *J. Chem. Phys.* **1997**, *107*, 5422.

(76) Bieske, E. J.; Nizkorodov, S. A.; Bennett, F.; Maier, J. P. *Int. J. Mass Spectrom. Ion Processes* **1995**, *150*, 167.

(77) Buck, U. *J. Phys. Chem.* **1994**, *98*, 5190.

(78) McIlroy, A.; Lascola, R.; Lovejoy, C. M.; Nesbitt, D. J. *J. Phys. Chem.* **1991**, *95*, 2636.

(79) Fraser, G. T.; Pine, A. S. *J. Chem. Phys.* **1986**, *85*, 2502.

(80) Hutson, J. M. *J. Chem. Phys.* **1992**, *96*, 6752.

(81) Liu, S. Y.; Bacic, Z.; Moskowitz, J. W.; Schmidt, K. E. *J. Chem. Phys.* **1994**, *101*, 10181.

(82) Liu, S. Y.; Bacic, Z.; Moskowitz, J. W.; Schmidt, K. E. *J. Chem. Phys.* **1994**, *100*, 7166.

(83) Stace, A. J. *J. Am. Chem. Soc.* **1984**, *106*, 4380.

(84) Engelking, P. C. *J. Chem. Phys.* **1986**, *85*, 3103.

(85) Klots, C. E. *J. Chem. Phys.* **1985**, *83*, 5854.